International Journal for Housing Science and Its Applications
Publish August 10, 2025. Volume 46, Issue 4 Pages 444-453

https://doi.org/10.70517/ijhsa46440

Research on Condition Monitoring Method of Conventional DC Converter Valve Based on Acoustic Signal Processing Algorithm

Yi Jiang[1,*], Jiashui Dai[1], Ao Feng[2], Qian Luo[1], Jianming Meng[1], Mukun Jin[1] and Baoji Xie[1]
[1] Tianshengqiao Bureau, Ultra-high Voltage Transmission Company of China Southern Power Grid Co., Ltd., LTD., Xingyi, Guizhou, 562400, China
[2] Wuhan University, Wuhan, Hubei, 430072, China
Corresponding authors: (e-mail: qscjll@163.com).

Abstract With the continuous development of high-voltage direct current (HVDC) transmission technology, the Conventional DC Converter Valve is becoming more and more important to maintain system stability. This paper proposes an integrated monitoring method based on acoustic signal processing and multimodal timing analysis. The DC maximum current time series feature model is constructed to extract the maximum current eigenvolume and other characteristics. The acoustic signal of the converter valve is collected by combining the homogeneous electrode acoustic detection device and digitized. The TimesNet time series analysis model is introduced to convert the two-dimensional depth characteristics of the time series to realize the accurate positioning of the commutator valve phase change abnormality and vibration noise. Research shows that when the power load is 400MW, the frequency of the converter valve sound signal is concentrated within 3kHz, and the frequency increases with the increase of power. During the monitoring process, the output current of the converter valve fluctuates abnormally in 2-3s, while the voltage fluctuates abnormally in that time. The voltage ripple adjusted according to the monitoring results re-maintained the coherent state.

Index Terms acoustic signal processing, Conventional DC Converter Valve, maximum current characteristics, homogeneous electrode acoustic detection, TimesNet model

I. Introduction

Conventional DC Converter Valve is a key device to realize the conversion of alternating current (AC) and direct current (DC) in direct current (DC) transmission system [1], [2]. It achieves the conversion of electrical energy forms with the help of precise control of power electronic devices [3]. Conventional DC Converter Valves are mainly composed of power electronic devices (like thyristors, insulated gate bipolar transistors, etc.), control system, triggering system, cooling system, and electrical connecting parts [4]-[6]. In the case of thyristor converter valves, multiple thyristors are connected in series and parallel to form a valve group, and the control system allows the thyristors to conduct and turn off according to a specific triggering sequence, thus realizing the conversion of alternating current (AC) to direct current (DC) [7]-[9]. According to the design standard of China's ultra-high voltage DC transmission project, the design life of DC transmission core equipment - converter valve is 40 years [10], [11]. How to timely and effectively monitor the various faults and hidden dangers of the equipment, such as the temperature, pressure, torque, and small leakage current of the key components of the converter valve, as well as the valve tower cooling pipeline leakage and other non-normal operating conditions, to provide a reliable basis for the operator to analyze and judge, to avoid the occurrence of accidents or further expansion of the important topic of the urgent need to seriously study and solve [12]-[15].

The traditional method of Conventional DC Converter Valve condition monitoring is mainly manual, and its monitoring effect is more subjective, which can not realize the condition monitoring completely accurately and timely, and is not conducive to the safe operation of the transmission system, while the acoustic signal processing algorithm, as an important branch of the artificial intelligence field, plays an important role in the state monitoring of the converter valve [16]-[19]. Acoustic signal processing algorithm is a technology that converts sound signals into digital signals and processes and analyzes them [20], [21]. It has a wide range of applications in audio processing, speech recognition, music synthesis and other fields [22]. The acoustic signal processing algorithm in the condition monitoring of the converter valve can realize accurate condition monitoring by extracting the vibration information for identification and localization [23]-[25].

This paper focuses on acoustic signal processing and multimodal time series analysis, and systematically elaborates the core method of converter valve condition monitoring. Modeling the timing characteristics of the DC

maximum current, analyzing the periodicity of the current waveform during the phase change process and the criteria of abnormality. The acoustic detection device of the equalizing electrode is designed to collect the vibration signals of the converter valve through the acoustic sensor, and realize the integrated processing of acoustic wave excitation, echo collection and signal conditioning. Aiming at the limitations of the traditional time series model, the TimesNet model is introduced to capture the multi-scale dependence of the time series through a two-dimensional convolutional network, and the time-frequency correlation characteristics of the acoustic signals are explored in depth.

II. Acoustic signal processing based on the realization of the state detection of the Conventional DC Converter Valve

II. A. Converter operation state modeling based on DC maximum current timing characteristics

II. A. 1) Constructing the DC maximum current eigenvolume

In order to reduce the influence of system operating conditions on the on-width and off-width, the ratio of the polarity current to the current at the intersection of the two commutator valves is used to construct the single-bridge DC maximum current eigenquantity S_m at the commutator port, with the criterion shown below:

$$S_m = \frac{i_{Vm}}{0.55 i_{ac\max}} = \frac{i_{Vm}}{0.55 \max\left(|i_a|,|i_b|,|i_c|\right)} \tag{1}$$

where, $i_{ac\max}$ is the absolute maximum of the three-phase DC currents i_a, i_b, i_c on the valve side of the converter, $0.55 i_{ac\max}$ is the current at the intersection point of the two commutator valves, and $|i_a|,|i_b|,|i_c|$ is the absolute value of the three-phase DC current on the valve side of the converter's single bridge.

The waveforms of S_m are different under normal operation and phase change abnormality:

(1) S_m consists of a discontinuous nearly trapezoidal waveform starting at the inverter-side trigger angle α_1 and terminating at $\alpha_1 + 125^\circ + \mu$, with a period of 360°, and an amplitude range of the non-zero region $(0.0, 2.0]$. Bounded by $S_m = 1.0$, S_m is the intersection of the hypotenuse of the trapezoidal wave at $S_m = 1.0$ occurs at the moment when the currents of the two valves of the commutated phase are equal. The width of the region at $S_m > 1.0$ is 125° and the width of the region at $S_m < 1.0$ is 245°.

2) The occurrence of phase change abnormality after a fault causes a change in the waveform of S_m. The S_m consists of discontinuous non-trapezoidal waveforms with different shapes, the original periodicity is broken, and the amplitude of the non-zero region decreases, resulting in an obvious change in the time width of the non-zero region. The appearance of the bypass pair completely destroys the normal conduction sequence of the converter valve, and the phase change process cannot be carried out smoothly. Phase change a in the commutator valve V4 to commutator valve V6 phase change is not completed, commutation failure occurs, S_4 although the amplitude has decreased, but has been at a high level, the long-term incomplete commutation caused by the non-zero region of the time width of the S_4 increased; On the contrary, although S_6 has increased in amplitude, the increase is small and short, and it is low for a long time, resulting in a decrease in the time width of the non-zero region of S_6.

During normal operation, the amplitude of $0.55 i_{ac\max}$ is half that of the AC current, and each AC maximum current eigenvolume S_m of the five valves is composed of the same waveform features and is periodic. At the phase change anomaly, the amplitude of $0.5 i_{ac\max}$ is no longer regular, and the amplitude of S_m is reduced, discontinuous and irregular. Therefore, the discrimination of the valve state can be realized by using the variation of the amplitude characteristics of S_m on the time series.

II. A. 2) Characterization of the AC maximum current eigenvolume

Valve virtual on state and virtual off state in distinguishing the converter normal phase change and abnormal phase change depends on whether the time width corresponding to each state is longer or shorter, and the key to longer or shorter on state and off state lies in the difference of the intersection point of the two valve currents of the phase change in the process of phase change, or whether there is a phase change intersection point.

The AC and DC currents at the two terminals of the converter are collected by the current transformer, which has nothing to do with the structure of the converter. As an example, the phase change process from valve V1 to valve V3 in the converter coupled to the YY transformer is used to analyze the characteristics of the polarity current in the phase change process. Figure 1 illustrates the equivalent circuit of the phase change from valve V1 to valve V3.

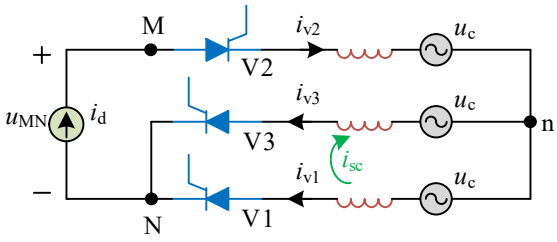

Figure 1: shows the equivalent circuit of commutating valve V1 to V3

The current flowing through the two valves of the phase change during the phase change is determined by the following equation:

$$\begin{cases} k_1 L_c \dfrac{di_{V3}}{dt} - k_1 L_c \dfrac{di_{V1}}{dt} = u_{ba} \\ u_{ba} = \sqrt{2} E_1 \sin(\omega t + \phi) \end{cases} \tag{2}$$

where, u_{ba} is the phase-change voltage, L_c is the equivalent phase-change inductance on the inverter side, k_1 is the transformer ratio on the inverter side, E_1 is the RMS value of the equivalent power line voltage on the inverter side, ω is the angular frequency of the system fundamental wave, ϕ is the angle of forward shift of the line voltage over zero point.

During the phase change process, the relationship between the current of the two phase change valves and the DC current is:

$$i_{V1} + i_{V3} = i_d = i_{dH} = i_{dN} \tag{3}$$

From Eqs. (2) and (3) and counting $i_{V3}(\alpha_I) = 0$, the current expressions for valves V1 and V3 of the phase change process are obtained:

$$\begin{cases} i_{V1} = i_d(t) - i_{V3} \\ i_{V3} = \dfrac{E_1}{\sqrt{2} k_1 \omega L_c} \left(\cos\alpha_I - \cos(\omega t + \phi) \right) \Big|_{t_1}^{t} + \dfrac{i_d(t) - i_d(t_1)}{2} \end{cases} \tag{4}$$

where, α_1 is the trigger delay angle on the inverter side; $t \in [t_1, t_2]$, t_1 is the beginning moment of valve V3 phase transition, $t_1 = (\pi - \beta)/\omega$, t_2 is the end moment of valve V3 phase transition, $t_2 = (\pi - \gamma - \phi)/\omega$.

When the currents flowing through the two valves of the phase change are equal $i_{V1} = i_{V3} = i_d(t_2)/2$, there must exist an intersection point θ_s of the phase change process, and the expression for this intersection point is:

$$\theta_s = \arccos\left(\cos\alpha_I - \frac{\sqrt{2} k_1 \omega L_c}{E_1} \left(\frac{i_d(t_2)}{2} - \frac{i_d(t_0) - i_d(t_1)}{2} \right) \right) - \alpha_I \tag{5}$$

where, t_0 is the moment of intersection, $t_0 = t_1 + \theta_s/16$.

The DC current can be calculated from the voltage across the DC line with the following expression:

$$\begin{cases} i_d = \dfrac{u_{dR} - u_{dI}}{R_d} = K_d \left(\dfrac{E_R}{k_R} \cos\alpha_R - \dfrac{E_I}{k_I} \cos\beta_I \right) \\ K_d = 6\sqrt{2} / (R_d \pi + 6\omega(L_c + L_R)) \end{cases} \tag{6}$$

where, u_{dR} is the rectifier ground voltage; k_R is the transformer ratio on the rectifier side; E_R is the RMS line voltage at the rectifier station; L_R is the equivalent inductance on the inverter side; u_{dI} is the inverter station voltage to ground; R_d is the DC resistance; α_R is the trigger delay angle on the rectifier side; β_I is the trigger overrun angle on the inverter side; and K_d is the coefficient.

Combining Eqs. (5) and (6), the phase change intersection point θ_s is mainly influenced by α_R, β_I, E_I and ϕ. When the system operates stably, the phase change process has equal phase change angles, the phase change intersection point θ_s is constant, the amplitude of S_m is certain and has a periodic law, and the valve's virtual on-width and virtual off-width are unchanged. After the system disturbance or fault, the amplitude of S_m will decrease, and the periodicity and regularity will change; the phase change intersection point θ_s is affected by the trigger angle and the phase change voltage, and will change before and after the fault, and the valve virtual on-state width and virtual off-state width will also change.

II. B.Acoustic testing of pressure equalizing electrodes

II. B. 1) Homogeneous electrode acoustic detection device design

Figure 2 shows the structure of the homogeneous pressure electrode acoustic detection experimental device. The field programmable gate array (FPGA) is used to control the acoustic excitation end and the acoustic receiving end, the piezoelectric transducer realizes the conversion of electro-acoustic energy and the focusing of acoustic energy under the action of the acoustic excitation end to form the acoustic wave interacting with the uniform pressure electrode, the acoustic receiving end collects the acoustic echo signals with the information of the scale layer, and then imports them into the PC for the characterization through the data transmission. According to the design process, the experimental device is mainly divided into three parts: acoustic excitation end, acoustic receiving end and FPGA control.

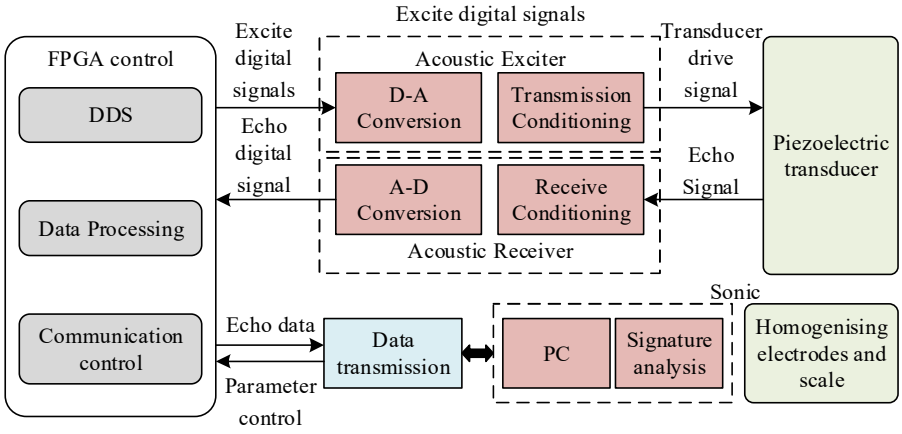

Figure 2: Structure of acoustic detection experimental device

The acoustic excitation end is responsible for converting the excitation digital signal synthesized by the FPGA into an analog signal, and the excitation signal is filtered, amplified and matched by the transmitter conditioning circuit to effectively drive the piezoelectric transducer to form an acoustic wave. The acoustic receiving end is responsible for receiving the echo signal from the transducer, which is amplified and filtered by the receiving conditioning circuit for signal amplification and noise reduction, and then converted to a digital signal through A-D, and received by the FPGA for caching.The FPGA control process serves as the core of the detecting device, which specifically includes a direct digital frequency synthesis (DDS) module for the generation of the excitation signals, a data processing module for the caching and cumulative averaging filtering of the echo data and a communication control module that controls the data transfer to interact with the PC.

II. B. 2) Stimulus end design

The selection of the center frequency directly determines the selection of ultrasonic transducer and detection effect. According to the theory of ultrasonic detection, to ensure the sensitivity of detection, the size of the detected object L should be at least greater than half of the acoustic wavelength λ, that is, it should be satisfied with the

$$L > \frac{\lambda}{2.0} = \frac{c}{2.0f} \tag{7}$$

For the case of this paper, the detected object is a fouling electrode, the electrode diameter l is 2.0 mm, and the thickness of the fouling layer is t, at which time $L = l + 2.0t$. Re-arrangement of equation (7), can be obtained as

$$f > \max\left(\frac{c}{2L}\right) = \frac{c_{se}}{2l} \approx 1.3\ MHz \tag{8}$$

In addition, the selected f should not be too large, otherwise it will exacerbate the attenuation of the return signal, so there should be a certain margin, this paper selects the center frequency of the excitation waveform as 1.55MHz.

In this paper, the excitation signal waveform is a sinusoidal pulse signal modulated by the Hanning window, and the number of cycles is 15 by default, which has better energy concentration under the excitation signal. In the actual detection, the center frequency and the number of cycles can be adjusted accordingly through the PC.

The excitation waveform data is pre-written into ROM, and the corresponding DDS module is enabled to read the ROM data through the decoding of the control module in the FPGA, thus outputting the excitation digital signal. AD9708 digital-to-analog converter chip is selected to convert the excitation digital signal into an analog signal, and at the same time, a seventh-order Butterworth low-pass filter circuit is used to remove the high-frequency noise in the converted output signal. Taking into account the low-pass filter circuit output voltage amplitude is low and can not effectively drive the piezoelectric transducer, it is selected AD8065 op-amp composition of the preamplifier circuit, and the low-pass filter output differential signal converted to a single-ended signal. Post-amplifier circuit using ADA4870 high-current drive amplifier, under the premise of ensuring portability, can be $\pm 25V$ dual power supply mode to achieve a maximum output amplitude of 38V, and the maximum drive current of 1.0A, suitable for the device used in the bicrystalline piezoelectric probe. At the same time, a low-pass L-shaped impedance matching circuit is used at the final stage output to match the equivalent load impedance after accessing the piezoelectric transducer to $50.0\,\Omega$ for maximum power transmission of the signal.

II. C. TimesNet

Traditional time series analysis methods have limitations in capturing long-term dependencies, so the TimesNet time series analysis model is proposed. A deep learning representation of time series data is achieved by converting a one-dimensional time series into a two-dimensional tensor and utilizing a deep neural network to capture the multi-scale patterns of temporal data.

II. C. 1) Variable conversion

TimesNet utilizes FFT to transform a one-dimensional time series into a two-dimensional tensor, and then captures its local and global dependencies efficiently with a two-dimensional convolutional network.

For a one-dimensional time series of length T, $X_{1D} \in \mathbb{R}^{T \times C}$, the time series is analyzed by FFT.

$$A = Avg\left(Amp(FFT(X_{1D}))\right) \tag{9}$$

$$\{f_1, \cdots, f_k\} = \arg Topk(A)$$
$$f_* \in \left\{1, \cdots, \left\lfloor \frac{T}{2} \right\rfloor\right\} \tag{10}$$

$$p_i = \left\lceil \frac{T}{f_i} \right\rceil, i \in \{1, \cdots, k\} \tag{11}$$

where $FFT(\cdot)$ and $Amp(\cdot)$ denote the computation of FFT and amplitude values. $\mathrm{Avg}(\cdot)$ denotes taking the average of the C dimensions to get the amplitude of each frequency $A \in \mathbb{R}^{T}$. TimesNet selects only the first k amplitude values to get the first k frequencies $\{f_1, \cdots, f_k\}$, and the length of the k most significant cycles is $\{p_1, \cdots, p_k\}$, the process can be summarized as:

$$A, \{f_1, \cdots, f_k\}, \{p_1, \cdots, p_k\} = Period(X_{1D}) \tag{12}$$

The one-dimensional time series $X_{1D} \in \mathbb{R}^{T \times C}$ is then reshaped into a plurality of two-dimensional tensors by Eq. (13).

$$X_{2D}^{i} = \mathrm{Re}\, shape_{p_i, f_i}\left(Padding\left(X_{1D}\right)\right) \quad i \in \{1, \cdots, k\} \tag{13}$$

where p_i and f_i denote the number of rows and columns of the transformed two-dimensional tensor, respectively, and $Padding(\cdot)$ denotes the addition of a zero value at the end of the time series so that it can be divisible by p_i. This results in a set of two-dimensional tensors $\left\{X_{2D}^{1}, X_{2D}^{2}, \cdots, X_{2D}^{k}\right\}$.

II. C. 2) Time blocks

TimesNet consists of a TimeBlock residual superposition. For a one-dimensional time series $X_{1D} \in \mathbb{R}^{T \times C}$ of length T, the original input is first projected into the deep feature $X_{1D}^{0} \in \mathbb{R}^{T \times d_{model}}$ model through the embedding layer $X_{1D}^{0} = Embed\left(X_{1D}\right)$. Then, for layer l of TimesNet, the input is $X_{1D}^{l-1} \in \mathbb{R}^{T \times d_{model}}$ and the output is:

$$X_{1D}^{l} = TimesBlock\left(X_{1D}^{l-1}\right) + X_{1D}^{l-1} \tag{14}$$

TimesNet consists of the following four sub-processes:

1) Conversion of one-dimensional time series to two-dimensional tensor

First, the input one-dimensional temporal feature X_{1D}^{l-1} is extracted and converted to a two-dimensional tensor $X_{2D}^{l,i}$. The conversion process is expressed in the following equation.

$$A^{l-1}, \{f_1, \cdots, f_k\}, \{p_1, \cdots, p_k\} = Period\left(X_{1D}^{l-1}\right) \tag{15}$$

$$X_{2D}^{l,i} = \mathrm{Re}\, shape_{p_i, f_i}\left(Padding\left(X_{1D}^{l-1}\right)\right) \quad i \in \{1, \cdots, k\} \tag{16}$$

2) Capturing 2D time-varying representation

Information is extracted using 2D convolution for a 2D tensor with 2D localization $\left\{X_{2D}^{l,1}, X_{2D}^{l,2}, \cdots, X_{2D}^{l,k}\right\}$. TimesNet uses the Inception model, viz:

$$\hat{X}_{2D}^{l,i} = Inception\left(X_{2D}^{l,i}\right) \tag{17}$$

3) Conversion of two-dimensional tensor to one-dimensional space

After capturing the temporal features, they are converted back to one-dimensional space for information aggregation.

$$\hat{X}_{1D}^{l,i} = Trunc\left(\mathrm{Re}\, shape_{1,(p_i \times f_i)}\left(\hat{X}_{2D}^{l,i}\right)\right) \quad i \in \{1, \cdots, k\} \tag{18}$$

where $\hat{X}_{1D}^{l,i} \in R^{T \times d_{model}}$, and $Trunc(\cdot)$ denotes the deletion of zeros that were added during the fill $(\cdot)$ operation in step (1).

4) Adaptive Aggregation

Finally, the adaptive aggregation mechanism is used to perform weighted summation of one-dimensional feature vectors. Adaptive fusion is to obtain a weighted sum of the one-dimensional representation $\left\{\hat{X}^{l,1}, \cdots, \hat{X}^{l,k}\right\}$ and output it according to the corresponding frequency values.

$$\hat{A}_{f_1}^{l-1}, \cdots, \hat{A}_{f_k}^{l-1} = Soft\max\left(A_{f_1}^{l-1}, \cdots, A_{f_k}^{l-1}\right) \tag{19}$$

Through the above steps, TimesNet is able to capture the fine-grained and multi-scale nature of its time-series data, achieving significant performance gains and multi-domain applications in time-series analysis tasks.

III. Based on acoustic signal processing, the monitoring practice of Conventional DC Converter Valve

III. A. Vibration and acoustic characteristics of value converter valves under different power loads

III. A. 1) Changes in the amplitude of the acoustic signal of a converter valve

In order to test the effectiveness of the method proposed in this paper for the condition monitoring of the converter valve, the converter valve used in a large-scale project is selected as the research object. Through the design of the even pressure electrode theological detection device, the collected current, voltage and other electrical signals are processed; combined with the TimesNet timing analysis model to process the time information of the electrical signals, and ultimately obtain the vibration and sound characteristics of the converter valve under different voltages, to verify the effectiveness of the method in this paper.

In order to study the changes generated by the vibration sound of the converter valve with the increase of voltage, the amplitude of the time-domain acoustic signals of the four monitoring points is plotted as a box-and-line diagram, and the upper and lower edges are about 1.25 times the standard deviation of the data. Figure 3 shows the time-domain sound signal amplitude at the monitoring points. The trend of sound changes at different measurement points is roughly the same. Figure 3 shows the amplitude of the time-domain acoustic signal at the monitoring points. The sound variation trends at different measurement points are approximately the same. When the power load is 200MW, the amplitudes of all measurement points are below 0.3V. At this time, the converter valve is in a normal critical state and generates relatively large vibration noise. As the voltage rises, the converter valve normal and abnormal state conversion accelerated, resulting in a high-frequency component of the vibration noise increased significantly, of which the measurement point 2 by the voltage growth of the influence of the larger, the acoustic signal amplitude change of more than 1.88 times. However, the converter valve vibration and voltage amplitude quadratic nonlinear relationship, when the power load reaches 400MW, the growth rate of the acoustic signal amplitude decreases, and gradually tends to level off.

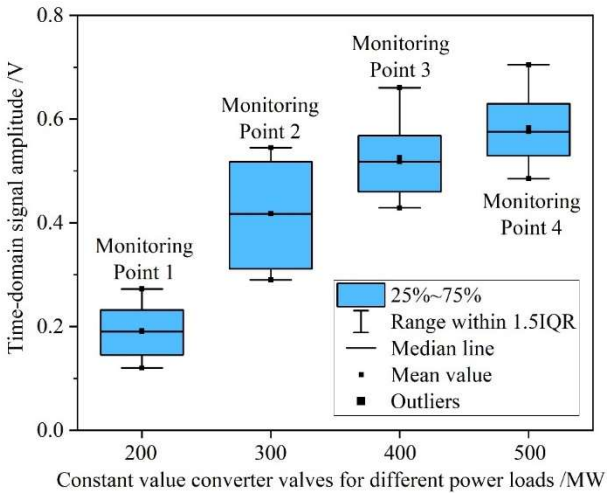

Figure 3: The variation of acoustic signal amplitude

III. A. 2) Frequency of acoustic ripple of constant value converter valve at different voltages

After completing the vibration and acoustic pattern test of the converter valve under different voltages, further analyzing the data from measurement points 1 to 4, it is found that the vibration and acoustic pattern spectra of the converter valve under each measurement point are relatively similar as a whole. Therefore, this paper only selects the data analysis results of the front measurement point 3 of the converter valve to show. The frequency of the acoustic signal in the range of 55 Hz ~ 15 kHz are reflected on the 55 times the frequency, mainly concentrated in 55 Hz ~ 10 kHz.

The voltage of the converter valve contains a large number of odd and even harmonics, which makes the converting process faster and more saturated, and the frequency of the vibration produced is not only an even multiple of the voltage harmonics. It also contains a large number of odd harmonics, and the frequency band is wider, which is also consistent with the results of theoretical analysis. Fig. 4 shows the frequency share of the vibration sound pattern at different voltages in the boosting test, and only the spectral distribution from 0 to 10 kHz is presented in the figure. When the power load is relatively low (200MW), the frequency is mainly concentrated

within the range of 3kHz; as the voltage rises, the low-frequency component gradually decreases, the high-frequency component keeps increasing, and the main frequency band is shifted toward the high-frequency direction. When the power load reaches 300MW, the frequency proportion within the range of 4-10kHz approaches that of 0-3kHz. As the power load continues to increase, the changing trend of each frequency band slows down.

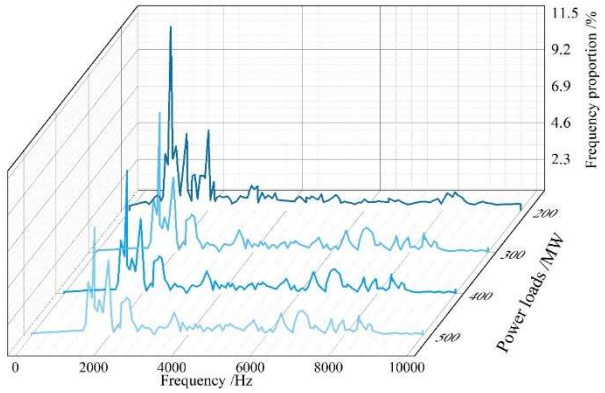

Figure 4: Proportion of Vibration voiceprint frequencies under Different power loads

III. B. Condition monitoring process of Conventional DC Converter Valve

III. B. 1) Current Waveform Reduction and Capacitor Voltage Change Analysis

Using the method of this paper, it is possible to visualize and analyze the effect of voltage changes on the sound pattern. Combined with the processed sound pattern characteristics, it can also restore the current changes during the operation of the converter valve. Figure 5 shows the super capacitor charging current and its local amplification in the converter valve during condition monitoring. Figure 6 shows the super capacitor voltage change process during the charging of the converter valve. The output current of the converter valve is basically maintained at about 2.0kA in 0-6s, and the up and down fluctuation of the current is no more than 0.01kA in most moments, and the current ripple is small. However, in some moments, such as between 2-3s, a short abnormal fluctuation occurs, resulting in a large increase in current ripple. Combined with the supercapacitor voltage during charging, it can be seen that the supercapacitor voltage fluctuates and grows linearly at a charging current of about 2.0 kA, and the capacitor voltage increases by about 1.18 kV in 6 s. Similarly, there are some moments of abnormal fluctuations during the growth of the capacitor voltage. For example, there is a flat fluctuation in 2-3s when there should be a large capacitor voltage fluctuation. Through the method of this paper, it can be determined that there are some moments of abnormal fluctuations in the working process of the converter valve, which need to be adjusted by the monitor according to the analysis results in order to maintain the stable operation of the converter valve.

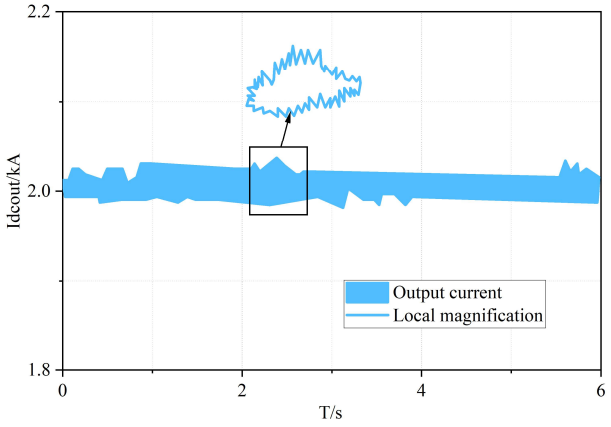

Figure 5: Charges current of supercapacitors and its local amplification situation

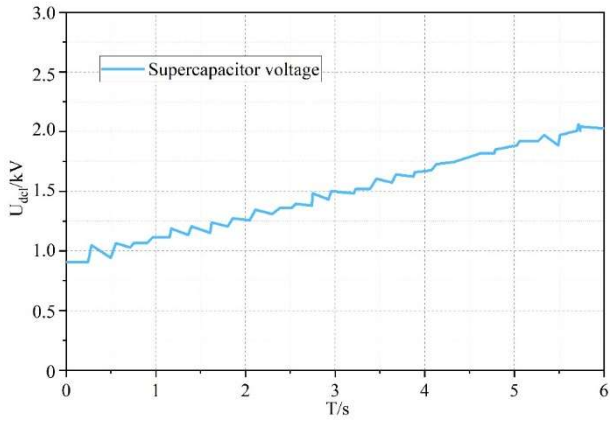

Figure 6: The supercapacitor voltage

III. B. 2) Control switching practices

The converter valve control switching performed by the monitor based on the monitoring results realizes the voltage and current adjustment by changing the resistance value of the resistor on the load side. Figure 7 shows the waveform comparison before and after switching. The 2-3s time period is divided into 6 compartments by 10ms order of magnitude, and the resistance is cast and cut in segments to adjust the capacitor voltage in the time period, so that it is kept in stable continuity. From the adjusted output voltage ripple, it can be seen that after adjustment according to the analysis results, the output voltage ripple changes from the original break to continuous, and the fluctuation amplitude in 2-3s is greatly reduced. This also verifies that the method of this paper can accurately process the acoustic signal, so as to determine whether the converter valve exists in an abnormal state at a certain moment, and assist the monitor to make corresponding adjustments.

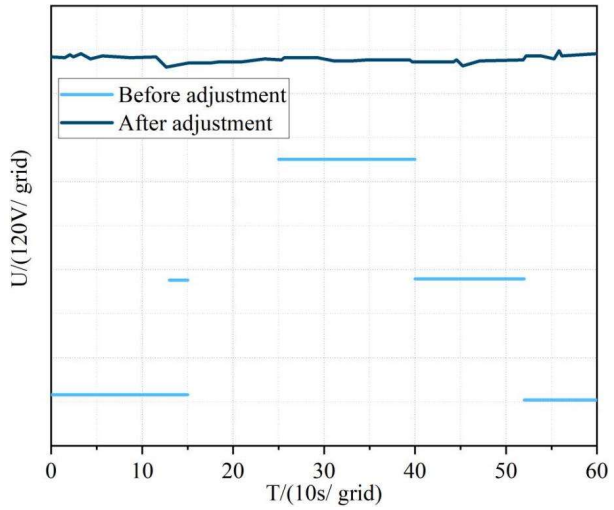

Figure 7: Waveform comparison before and after switching

IV. Conclusion

This paper proposes a state monitoring method of Conventional DC Converter Valve based on acoustic signal processing and TimesNet model to realize the synergistic diagnosis of phase change abnormality and vibration noise. The vibration noise of the converter valve is converted from the critical edge to abnormal change during the power load growth from 200MW to 500MW, and the growth rate tends to slow down. The actual monitoring found that in 0-6s, the output current of the Conventional DC Converter Valve stays above and below 2.0kA, and the fluctuation amplitude is less than 0.01kA and the current ripple is small. The current and voltage in the time period of 2-3s in which an abnormal state exists fluctuate abnormally at the same time and need to be adjusted manually. In the future, the lightweight network structure can be combined to improve the signal processing speed of the monitoring system and its real-time performance.

Funding

This work was supported by the Science and Technology Project of China Southern Power Grid Company Limited under (CGYKJXM20220335).

References

[1] Tang, G., He, Z., & Pang, H. (2014). R&D and application of voltage sourced converter based high voltage direct current engineering technology in China. Journal of Modern Power Systems and Clean Energy, 2(1), 1-15.

[2] Ning, Z., Wang, C., Deng, W., & Zhang, K. (2019, January). Study of the heavy direct current indirect measurement and calculation based on the waveform measuring of valve currents. In AIP Conference Proceedings (Vol. 2066, No. 1). AIP Publishing.

[3] Wei, Z., Yuan, Y., Lei, X., Wang, H., Sun, G., & Sun, Y. (2014). Direct-current predictive control strategy for inhibiting commutation failure in HVDC converter. IEEE Transactions on Power Systems, 29(5), 2409-2417.

[4] Liu, Z., Yu, J., Guo, X., Sun, T., & Zhang, J. (2015). Survey of technologies of line commutated converter based high voltage direct current transmission in China. CSEE Journal of Power and Energy Systems, 1(2), 1-8.

[5] Shahin, R. G., & Al-Majali, H. D. (2022). Performance analysis of multi-level high voltage direct current converter. International Journal of Electrical and Computer Engineering (IJECE), 12(2), 1368-1376.

[6] Liu, H., Guo, H., Tan, M., Li, Q., Meng, X., & Yang, X. (2022). Accurate optical fiber current transducer for high-voltage direct current (HVDC) transmission. Instrumentation Science & Technology, 50(6), 604-615.

[7] Nho, E. C., Han, B. M., Chung, Y. H., Baek, S. T., & Jung, J. H. (2013). Synthetic test circuit for thyristor valve in HVDC converter with new high-current source. IEEE Transactions on Power Electronics, 29(7), 3290-3296.

[8] Gou, R. (2019). Research on 1100-kV/5500-A ultra-high voltage thyristor valve key technology and its application. IEEE Transactions on Power Electronics, 34(11), 10524-10533.

[9] Yue, K., Pang, L., You, H., Li, S., Kong, D., Li, Y., ... & Liu, L. (2017). Reverse recovery characteristics of high power thyristors in HVDC converter valve. IEEE Transactions on Dielectrics and Electrical Insulation, 24(4), 2132-2140.

[10] Bang, S., Kim, H. S., Koo, J. H., & Lee, B. W. (2021). Consideration of the insulation design method on a±200 kV converter valve unit in an HVDC converter hall. Energies, 14(8), 2296.

[11] Thind, B. S., Thomas, A. J., & Reddy, C. C. (2020). Effect of voltage waveforms of HVDC converter transformer on lifetime characteristics. IEEE Transactions on Power Delivery, 36(5), 3101-3108.

[12] Liu, K., Tang, J. K., Wang, Z., Guo, J. B., yuan Yang, G., Liang, N., & Zou, Y. S. (2019). The application of a novel infrared temperature measurement system in HVDC converter valve equipment connector overheat failure prevention. Procedia Computer Science, 154, 267-273.

[13] Yu, H., Xu, M., Peng, L., Wang, H., & Hou, Z. (2020). Research on Abnormal Condition Monitoring System of UHV Converter Valve Based on Infrared/UV Image. In Advances in 3D Image and Graphics Representation, Analysis, Computing and Information Technology: Algorithms and Applications, Proceedings of IC3DIT 2019, Volume 2 (pp. 393-399). Singapore: Springer Singapore.

[14] Maalla, A. (2020, June). Current Status of Valve Base Electronics Equipment in DC Transmission System. In 2020 IEEE 5th Information Technology and Mechatronics Engineering Conference (ITOEC) (pp. 1809-1812). IEEE.

[15] Dai, J., Tan, F., Jiang, Y., Liang, Y., Lin, K., & Tong, K. (2025). Infrared image monitoring algorithm for converter valve equipment. AIP Advances, 15(3).

[16] Du, F., Chang, W., Wang, G., Yuan, S., & Gong, Y. (2022, December). Key Parameters of Electromagnetic Compatibility of On-line Monitoring Sensor Device for Power Converter Valve. In Journal of Physics: Conference Series (Vol. 2378, No. 1, p. 012002). IOP Publishing.

[17] Rui, Y., Yunpeng, L., Jianghai, G., Yimiao, W., Yuling, L., & Lin, Z. (2025). Detection of Partial Discharge Acoustic Signals in Converter Valve Halls Using Multivariate Time-Frequency Slices. IEEE Sensors Journal.

[18] Guo, J., Liu, H., Feng, L., & Zu, L. (2024). A fault diagnosis method for flexible converter valve equipment based on DSC-BIGRU-MA. Frontiers in Energy Research, 12, 1369360.

[19] Bi, Y., Liu, K., Yang, H., & Qiu, W. (2024, March). Development of SyntheticTest System for Thyristor Voltage Monitoring of Converter Valve. In Journal of Physics: Conference Series (Vol. 2717, No. 1, p. 012045). IOP Publishing.

[20] Chaki, J. (2021). Pattern analysis based acoustic signal processing: a survey of the state-of-art. International Journal of Speech Technology, 24(4), 913-955.

[21] Guo, M., Ma, Y., Yang, X., & Mankin, R. W. (2019). Detection of damaged wheat kernels using an impact acoustic signal processing technique based on Gaussian modelling and an improved extreme learning machine algorithm. biosystems engineering, 184, 37-44.

[22] Zhao, L., Kang, L., & Yao, S. (2018). Research and application of acoustic emission signal processing technology. Ieee Access, 7, 984-993.

[23] Rajapaksha, N., Jayasinghe, S., Enshaei, H., & Jayarathne, N. (2021, December). Acoustic analysis based condition monitoring of induction motors: A review. In 2021 IEEE southern power electronics conference (SPEC) (pp. 1-10). IEEE.

[24] Mc Caffrey, C., Sillanpää, T., Huovila, H., Nikunen, J., Hakulinen, S., & Pursula, P. (2017). Energy autonomous wireless valve leakage monitoring system with acoustic emission sensor. IEEE Transactions on Circuits and Systems I: Regular Papers, 64(11), 2884-2893.

[25] Ali, Y. H., Abd Rahman, R., & Hamzah, R. I. R. (2014). Acoustic emission signal analysis and artificial intelligence techniques in machine condition monitoring and fault diagnosis: a review. Jurnal Teknologi (Sciences & Engineering), 69(2).